ACS APPLIED MATERIALS & INTERFACES

Research Article

www.acsami.org

Catalytic, Self-Cleaning Surface with Stable Superhydrophobic Properties: Printed Polydimethylsiloxane (PDMS) Arrays Embedded with TiO_2 Nanoparticles

Yuanyuan Zhao,[†,‡] Yang Liu,[†,‡] Qianfeng Xu,[†] Mark Barahman,[†] and Alan M. Lyons*[,†,‡]

[†]Department of Chemistry, College of Staten Island, City University of New York, Staten Island, New York 10314, United States
[‡]The Graduate Center, City University of New York, 365 Fifth Avenue, New York, New York 10016, United States

Supporting Information

ABSTRACT: Maintaining the long-term stability of superhydrophobic surfaces is challenging because of contamination from organic molecules and proteins that render the surface hydrophilic. Reactive oxygen species generated on a photocatalyst, such as TiO_2, could mitigate this effect by oxidizing these contaminants. However, incorporation of such catalyst particles into a superhydrophobic surface is challenging because the particles become hydrophilic under UV exposure, causing the surface to transition to the Wenzel state. Here we show that a high concentration of hydrophilic TiO_2 catalytic nanoparticles can be incorporated into a superhydrophobic surface by partially embedding the particles into a printed array of high aspect ratio polydimethylsiloxane posts. A stable Cassie state was maintained on these surfaces, even under UV irradiation, because of the significant degree of hierarchical roughness. By printing the surface on a porous support, oxygen could be flowed through the plastron, resulting in higher photooxidation rates relative to a static ambient. Rhodamine B and bovine serum albumin were photooxidized both in solution and after drying onto these TiO_2-containing surfaces, and the effects of particle location and plastron gas composition were studied in static and flowing gas environments. This approach may prove useful for water purification, medical devices, and other applications where Cassie stability is required in the presence of organic compounds.

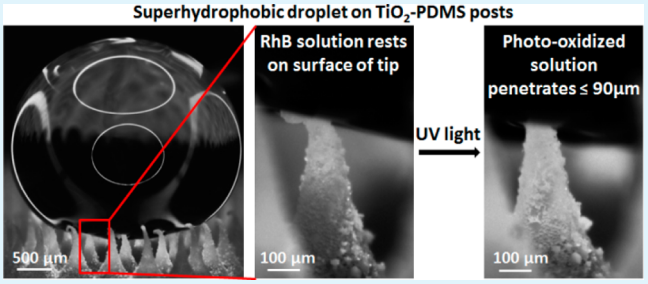

KEYWORDS: *photocatalytic surface, rhodamine B, solid−liquid−gas interface, printing, wetting*

INTRODUCTION

Superhydrophobic surfaces have been fabricated using a wide range of techniques,[1−4] including photolithography,[5−7] sputter deposition,[8] casting of nanoparticle−polymer films,[9] templating,[10−13] ion assisted deposition on porous Teflon membranes,[14] and chemical vapor deposition.[15,16] One challenge to using these superhydrophobic surfaces is that the stability of the Cassie state may be compromised by contamination from organic molecules and proteins.[8,17] Only a few surfaces have been reported that are omniphobic[18−20] and fewer still that are resistant to protein deposition.[21] As these surfaces are fragile and expensive to fabricate, alternative approaches are necessary. Supporting fluid in the Cassie state, even if the surfaces are coated with protein, is not ideal for medical applications or where the surfaces are intended for long-term use because protein coated surfaces foster the growth of bacteria and the formation of biofilms that may cause infections[22] as well as the loss of superhydrophobicity.

One approach to fabricating a stable superhydrophobic surface and preventing the accumulation of organic contaminants is to augment the functionality of the surfaces by incorporating catalytic materials on which reactive oxygen species (ROS), such as superoxides, hydroperoxides, or singlet oxygen, are photogenerated. Such ROS oxidize organic compounds leading to their decomposition into smaller molecules and ultimately a clean surface. Indeed, we have recently reported on the fabrication and properties of superhydrophobic surfaces that incorporate hydrophobic silicon−phthalocyanine glass particles that generate singlet oxygen in both the plastron and in solution.[23,24] Also, surfaces incorporating hydrophobic rare-earth metal oxides have been reported.[25] Although these are potentially valuable systems, incorporation of specialty catalyst materials may prove too expensive and/or toxic to meet the needs of medical devices or large scale water purification and waste-treatment applications.

Many studies have focused on the fabrication of superhydrophobic surfaces using common metal oxide catalysts such as TiO_2,[8,9,14,16,26−28] although other metal oxides have been studied including ZnO [29] and V_2O_5.[30] In many cases the oxide surface must be modified (e.g., with a silane) to achieve superhydrophobicity due to the relatively high surface energy of the oxides.[26,31] However, the photooxidation of this chemical

Received: November 4, 2014
Accepted: December 19, 2014
Published: December 19, 2014

DOI: 10.1021/am5076315
ACS Appl. Mater. Interfaces 2015, 7, 2632−2640

treatment becomes catalyzed by the particle and the surface permanently loses its superhydrophobicity under UV light.[31] Surfaces composed of hydrophilic metal oxides with sufficient roughness and/or surfaces with re-entrant topographies are able to maintain superhydrophobicity without the aid of silane surface treatments.[27,28] However, these surfaces exhibit a reversible wetting transition. Upon exposure to UV light, the oxide surface energy increases and the liquid will transition from the Cassie to the Wenzel state.[27,28] Surfaces incorporating TiO_2 particles dispersed in a polymer matrix have been reported[8,16] that exhibit a stable Cassie state when exposed to UV light only when the concentration of TiO_2 is sufficiently low. Although the photooxidation of organic dyes was reported, the rates were slow[8] or the catalytic measurements were only conducted on the surface when it was in a fully wetted Wenzel state.[16]

One of the potential advantages of catalytic superhydrophobic surfaces is that a layer of gas exists between the substrate and the liquid, known as the plastron. By control of the composition of the gas at this solid−liquid−gas (triphasic) interface, superhydrophobic surfaces could be uniquely well suited for fundamental studies of heterogeneous catalytic reactions. The photocatalytic superhydrophobic surfaces previously reported have been created on solid, rigid substrates that provide no access to the plastron.[8,16] For reactions involving a gaseous reactant, such as TiO_2 photooxidation reactions, the lack of plastron access limits the utility of such superhydrophobic surfaces. These requirements demonstrate the need for a new approach to fabricate superhydrophobic surfaces composed of catalytic particles with high photooxidation efficiency, stable superhydrophobicity, and facile access to the plastron.

Here we present a novel method for preparing superhydrophobic surfaces composed of catalytic metal oxide particles where no surface treatment is required to achieve superhydrophobicity. The particles are partially embedded into printed arrays of polydimethylsiloxane (PDMS) posts. This approach ensures that a relatively high catalyst surface area is in direct contact with an aqueous solution maintained in the Cassie state. Superhydrophobicity is achieved, even with hydrophilic catalytic particles, because of significant hierarchical roughness. Catalyst particles can be synthesized by any process, and so commodity TiO_2 nanoparticles (e.g., P25 from Evonik) can be used as well as visible light active catalyst particles[32] that are prepared under elevated temperatures and/or pressures. By separation of the catalyst synthesis step from the superhydrophobic surface fabrication process, superhydrophobic catalytic films can be formed using a facile, scalable method at ambient pressure and modest temperatures.

Another important feature of the high aspect ratio primary roughness is that it enables easy access to the plastron. Printing the PDMS posts on a porous membrane, and supporting the membrane over a plenum, provides a means to control the composition of the gas in the plastron and thus study catalysis at the solid−liquid−gas interface. In this paper, we demonstrate the photocatalytic degradation of rhodamine B (RhB) as a function of plastron gas composition using TiO_2 nanoparticles disposed on the surface of PDMS posts. The self-cleaning property of this TiO_2−PDMS surface was also studied using fluorescently labeled BSA protein as a model contaminant.

EXPERIMENTAL SECTION

Reagents, Materials, and Instrumentation. A room-temperature vulcanizing (RTV) hydroxy-terminated dimethylsiloxane, manufactured by Dow Corning and sold as DAP clear aquarium silicone sealant 688, was used to print PDMS superhydrophobic surfaces. TiO_2 nanoparticles were received from Evonik (P25 with nominal particle diameter of 21 nm), and SiO_2 particles (with nominal aggregate size of 300 nm) were from Cabot (TS-530). RhB was purchased from Acros Organics. BSA Alexa Fluor 488 conjugate was purchased from Life Technologies. The above chemicals were used as received without further purification. Deionized water (18 MΩ) was purified using Millipore Quantum filtration system with 0.22 μm filter.

A robot (Janome-2203N) was used as the PDMS dispenser. Optical energy was delivered from a Dymax Blue Wave 200 UV lamp (280−500 nm) with a mercury bulb and main peaks at 365, 405, and 436 nm. The UV light intensity (12 or 4 mW/cm^2) was measured with a Dymax Smart UV intensity meter (ACCU-ACL-50, measuring UV irradiation in the range from 320 to 395 nm). A liquid-filled optical waveguide (5 mm diameter) from the light source was brought into the cuvette with an incident angle of 90° to the surface. A ramé-hart model 250 goniometer with a motorized stage was used to measure contact angles and slip angles. Scanning electron microscopy (SEM) images were obtained using AMRAY 1910 field emission scanning electron microscope. Confocal images were taken by Leica SP2 AOBS confocal microscope. IMARIS software was used to calculate fluorescence intensity and reconstruct 3D surface images.

Preparation of Catalytic PDMS Posts. The process for printing PDMS posts was reported previously.[24,33,34] Briefly, the PDMS posts were printed as a 17 × 17 square array with a pitch of 0.5 mm (8 mm × 8 mm array, 1 mm tall) on a 10 mm × 10 mm membrane surface. Nanoparticles were spread onto the posts immediately after printing, and then the surface was cured at 60 °C for 120 min. The viscous and thixotropic properties of the PDMS maintained their shape before cure; the particles became partially embedded into the uncured surface, ensuring good adhesion between the particles and the PDMS posts. Excess particles were removed by exposing the surface to high flows of compressed air and rinsed with deionized water.

To assess the effect of solution contact with TiO_2 particles, surfaces were also prepared where the TiO_2 particles were isolated in the plastron. A surface completely coated with TiO_2 nanoparticles was first prepared, then modified by dipping the fully TiO_2 coated PDMS post surface into a thin layer of uncured silicone (Corning 3140), dusted with SiO_2 nanoparticles (Cabot TS530), followed by curing at 60 °C for 2 h. The upper portion of the PDMS posts (~200 μm) was covered by SiO_2, and the lower part of the posts (~800 μm) was covered by TiO_2. Control surfaces were fabricated by coating the PDMS post with only SiO_2 nanoparticles.

Contact and Slip Angle Measurements. A 20 μL droplet of deionized water was carefully placed on top of the surface to measure the static contact angle. On this type of superhydrophobic surface, the slip angle was defined as the angle required to displace the droplet by two posts (1 mm) in both the advancing and receding directions. At least 10 measurements were made for each sample. The surface was dried after each measurement by blowing high-pressure, dry, filtered air for approximately 5 s.

Device Fabrication and Procedure for Photocatalytic Reactions. For the plastron gas experiments, a three-phase photoreactor was constructed. A similar procedure was used as described previously[24] and is summarized here. The bottom of a PMMA disposable cuvette was removed to enable connection to the superhydrophobic photocatalytic surface. TiO_2−PDMS posts were printed onto a Millipore membrane (10 mm × 10 mm) with a pore size of 0.5 μm, coated with TiO_2 nanoparticles, and cured. The printed membrane was then placed on a 1 cm^2 × 2 mm thick Delrin support plate which defined the top of the plenum. Five holes (1 mm diameter each) drilled through the plate enable gas flow from the plenum through the membrane to the plastron. The support plate was inserted halfway into a 1 cm^2 custom-molded silicone rubber chamber (3 mm thick), leaving a 1.5 mm deep plenum for gas purging. A 25G 1 $^1/_2$′

DOI: 10.1021/am5076315
ACS Appl. Mater. Interfaces 2015, 7, 2632−2640

needle was bent and inserted into the bottom of the plenum with the silicone forming a gastight seal. The other end of the needle was connected to a regulated gas supply; the gas flow rate was controlled with a rotometer. One bubble was released every 2 s. To prevent the wetting of side wall posts by the solution, the bottom inner sides (0.5 mm × 0.8 mm for each side) of the cuvette were first coated by silicone (Corning 3140) and then dusted with SiO_2 nanoparticles to render the lower portion of the cuvette superhydrophobic. After curing at 60 °C for 2 h, excess particles were removed by washing under deionized water and compressed air. The cuvette was placed in an Ocean Optics cuvette holder fitted with optical fibers connected to a light source (Mikropack HL2000) and spectrometer (Ocean Optics USB4000) such that the solution absorption spectrum could be measured in situ during UV irradiation from the top of the cuvette. In some cases, UV−visible spectra were collected using a PerkinElmer (Lambda 650) spectrophotometer.

Self-Cleaning Demonstration. Both TiO_2−PDMS and SiO_2−PDMS surfaces were immersed into a BSA Alexa Fluor 488 solution (30 μg/mL) for 60 min. Surfaces were then rinsed with deionized water and dried with compressed air. The dried surfaces were exposed to UV light (150 mW/cm^2) for 2 h. Confocal images were taken before and after UV exposure. The excitation wavelength was 488 nm, and the fluorescence window was 498−540 nm. The posts were scanned over an absolute height of 300 μm at an interval of 1.2 μm between scans for a total of 250 scans.

Photodegradation Activity of TiO_2 Dispersion in RhB Aqueous Solution. TiO_2 nanoparticles (0.5 g, P25 from Evonik) were dispersed in 100 mL of RhB solution (10 mg/L) in a 250 mL Pyrex beaker. The photocatalytic reaction was conducted under UV light (Dymax Blue Wave 200, 12 mW/cm^2) for 1 h with stirring (500 rpm). To measure the concentration of RhB, 1 mL of the solution was removed from the reaction mixture at 15 min intervals and centrifuged. After centrifugation, the absorbance of the supernate was measured at 554 nm using a PerkinElmer Lambda 650 UV−vis spectrometer.

RESULTS AND DISCUSSION

Surface Microstructure and Superhydrophobicity. The printing process forms a substrate with an array of high aspect ratio (1 mm tall × 0.5 mm diameter × 0.5 mm pitch) PDMS posts that define the primary roughness of the surface. These posts are coated with a layer of TiO_2 nanoparticles that are partially embedded into the PDMS surface. Figure 1 shows

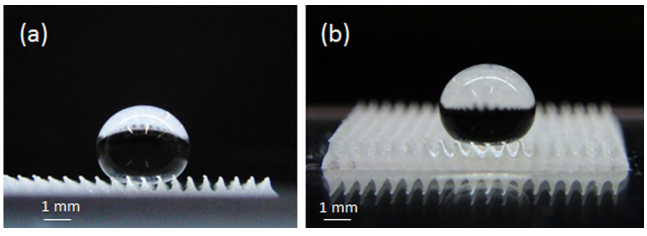

Figure 1. A 1 cm × 1 cm array of printed PDMS posts coated with TiO_2 nanoparticles with a 20 μL water droplet posed on the surface as seen from (a) side view and (b) perspective view.

optical images of a 1 cm × 1 cm array with a 20 μL water droplet on the surface. The TiO_2 particles form agglomerates of approximately 200 nm diameter (secondary roughness), which are approximately 10 times larger than the 20−25 nm individual particles that form the tertiary roughness. The microstructure of the TiO_2−PDMS surface is shown in the SEM images (Figure 2a−c). It is this hierarchical roughness (post, agglomerates, and individual nanoparticles), where the relatively course agglomerates of nanoparticles form a re-entrant surface geometry,[18,19] that maintains aqueous liquids in a stable Cassie state (Figure 2d, Figure 2e).

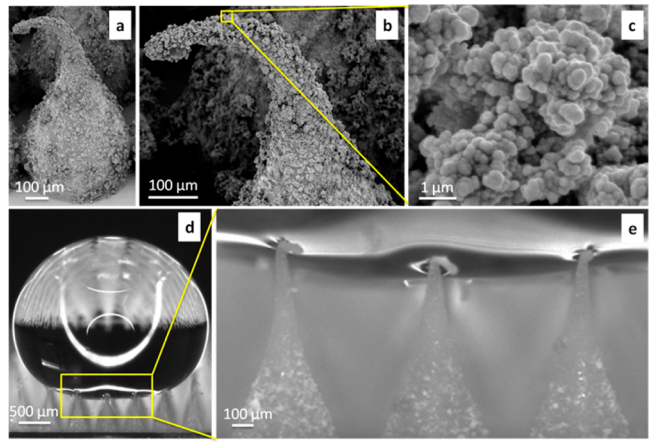

Figure 2. SEM images of a PDMS post partially embedded with TiO_2 nanoparticles and optical microscope images of a 20 μL water drop on the printed surface: (a) whole post; (b) high magnification of a post tip; (c) higher magnification showing TiO_2 nanoparticle agglomerates; (d) optical image of a 20 μL water drop on a printed surface; (e) enlarged image of the solid−liquid−gas interface illustrating how the liquid surface deforms about the nanoparticles.

The contact angle of a 20 μL water droplet on a freshly prepared TiO_2−PDMS surface is 162° ± 5°, and the slip angle was measured to 5° ± 1°. The high contact angle and low slip angle indicate minimal chemical and physical interaction between the liquid and the solid surface, resulting in a short and discontinuous triple contact line, consistent with observations. The surface of the droplet deforms about the TiO_2 coated tip surface as shown in Figure 2e.

For our printed hierarchical TiO_2−PDMS surfaces, water is supported in the Cassie state even when the TiO_2 particles become hydrophilic. After curing, the TiO_2 surface is hydrophobic. However, the surface of these anhydrous TiO_2 particles becomes hydrophilic when exposed to UV light in the presence of water[11,14,27,28] because of the formation of Ti−OH groups.[35] The initial hydrophobicity of TiO_2 could also be due to hydrophobic materials absorbed onto the surface; for example, low surface energy oligomers of PDMS could wet the nanoparticles during cure. Such groups would be photo-oxidized by UV light, rendering the surface hydrophilic.[31] The rapid rates of photo-oxidation, discussed in the next section, demonstrate that the TiO_2 surface must be in direct contact with the solution. Over a 3 h UV exposure (4 mW/cm^2), the position of the water−air interface descends only a small amount (<90 μm) into the plastron as shown in Figure 3a−d. At the later stages of this process, some PDMS post tips transitioned from the liquid−air interface into the liquid phase because of the increase in the hydrophilicity of the TiO_2 surface. However, the superhydrophobic properties remained stable with a fully intact plastron for two reasons: the TiO_2 particles away from the solid−liquid−air triple contact line (TCL) remain relatively hydrophobic, and the overall length of the TCL increases as the interface descends because of the conical shape of the posts. The longer TCL increases the total force required for the droplet to advance and so helps to prevent further encroachment into the plastron. Close-up images of a single post, which partially supports a droplet before and after UV irradiation, are shown in Figure 3e−h. Initially, the droplet surface rests on the top edge of the post for both water and 10 mg/L RhB solution droplets as shown in Figure 3e and Figure 3g. The post tips are bent under the

DOI: 10.1021/am5076315
ACS Appl. Mater. Interfaces 2015, 7, 2632−2640

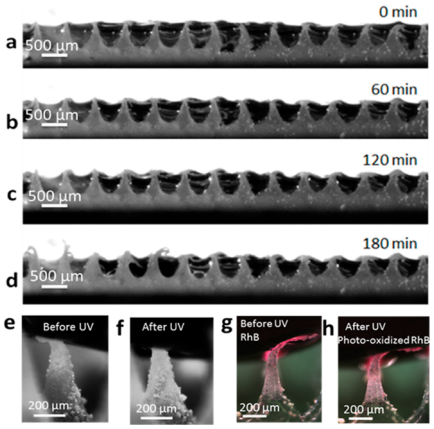

Figure 3. Optical images of the liquid–air interface position supported on a TiO_2–PDMS post surface as a function of UV irradiation time: UV irradiation time of (a) 0, (b) 60, (c) 120, and (d) 180 min. A 3 mm deep water layer rests across the surface (white). The plastron appears dark gray, and the PDMS posts appear light gray. (e) and (f) are close-up images of a single post which partially supports a 15 μL droplet of water before and after 180 min of UV irradiation. (g) and (h) are images of a single post which partially supports a 15 μL droplet of 10 mg/L RhB solution before and after the surface was irradiated for 120 min of UV irradiation.

weight of the droplet. After UV irradiation in contact with water, posts are shown to penetrate ~90 μm into the droplets (Figure 3f and Figure 3h) because of the increased hydrophilicity of the TiO_2 coated tips.

Photocatalytic Reactions. The three-phase catalytic chemical reactor device is shown schematically in Figure 4.

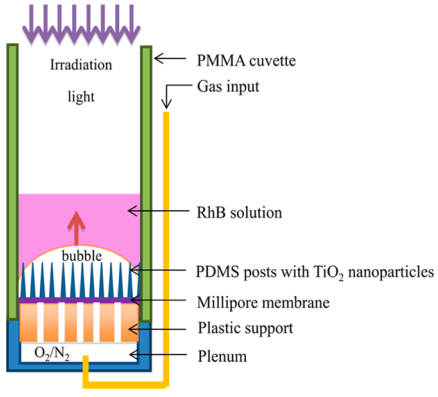

Figure 4. Schematic drawing of the cuvette reactor with a gas bubble formed on the surface.

This design enables the simultaneous irradiation of the catalyst and the monitoring of the solution concentration by UV–vis spectroscopy. In addition, a gas can be introduced into the plenum supporting the printed superhydrophobic surface such that it flows through the membrane and into the plastron. As shown in Figure 5 and Supporting Information video, bubbles formed at the plastron–liquid interface release and rise through the 2 mL of solution, increasing both the surface area and time over which the gas can dissolve into solution. After bubble release, a planar plastron re-forms and the bubble sequence repeats. The solution remains in the Cassie state throughout the experiment.

Decoloration of a RhB solution, monitored as a function of irradiation time, is shown in Figure 6. The reaction was conducted under flowing oxygen (20 cc/min). The concentration of RhB (10 mg/L) decreased by 80.0% after 3.5 h of irradiation with a rate constant of 0.0079 min^{-1} (Figure 7). First order kinetics was observed; a plot of ln[RhB] vs time was linear ($R^2 \geq 0.97$; Figure 7b), which is consistent with a Langmuir–Hinshelwood mechanism.[36,37]

Figure 8 shows the effect of plastron gas composition and flow condition on the photooxidation of the RhB solution. When the gas in the plastron was composed of static air, the rate of RhB decolorization was 0.0036 min^{-1}. Flowing O_2 through the plastron resulted in a RhB photooxidation rate of 0.0079 min^{-1}, which is 2.2 times faster than the rate in static air. Flowing N_2 reduced the photooxidation rate of RhB to 0.0008 min^{-1}, which is 89% slower than in flowing O_2. However, the rate was not reduced to zero. This low rate may be due to trace O_2 and/or hydroxyl radicals generated by the photocatalytic decomposition of water.[32] In a cuvette without any surface or TiO_2 particles present, the RhB concentration change was less than 0.3%. These results clearly show the need for both TiO_2 particles and high oxygen concentrations.

Flowing oxygen gas through the surface accelerated the photo-oxidation reaction not only because it ensured that the solution was saturated with oxygen but also because it induced mixing within the cuvette. Acceleration of the photo-oxidation rate due to mixing was confirmed by comparing the reaction rate under static air with air flowing through the solution. The variability of the RhB photooxidation rate was greater on surfaces under flowing O_2 than under static air or flowing N_2 as indicated by the relatively large error bars in Figure 8. This occurred because oxygen bubbles may exit from different locations across the PDMS post surface for each experiment, affecting the liquid–solid contact area under irradiation.

When compared to previously reported TiO_2 films, our printed TiO_2–PDMS surface exhibits a significant improvement; the normalized rate of RhB degradation is 9 times faster than the degradation of MB on a superhydrophobic TiO_2–PTFE nanocomposite film[8] after normalizing for UV power density and is twice the rate on the hydrophilic TiO_2–Ti nanocomposite film.[8] Since the relative rate of MB photooxidation by TiO_2 is higher than for RhB under the same experimental conditions,[40,41] the rate advantage for our TiO_2–PDMS surface over the TiO_2–PTFE nanocomposite would be expected to be even greater. The faster rate observed on the TiO_2–PDMS printed surface reflects the larger TiO_2 particle surface area in contact with the aqueous solution as well as the higher concentration of O_2 in solution near the surface.

This high rate of RhB decolorization on the TiO_2–PDMS surface in flowing O_2 approaches the rate when TiO_2 nanoparticles are dispersed directly into RhB solutions as shown in Table 1. Although direct comparison between TiO_2 coated surfaces and dispersions of nanoparticles is problematic because of the large number of experimental variables (e.g., particle and RhB concentration, stirring rate, wavelength distribution of light, UV power, etc.), relative rates can be compared. In our experiments, the TiO_2 dispersion is only 1.6 times faster than the TiO_2–PDMS surface. Rates for nanoparticle dispersions reported in the literature[38,39] appear to be slower than our surface.

The importance of solution–TiO_2 contact area is shown by comparing the RhB decomposition rates on the TiO_2–PDMS surface in the superhydrophobic (Cassie) state to when the solution is in the fully wetted (Wenzel) state. As shown in Figure 9, complete wetting led to a higher percentage of RhB

DOI: 10.1021/am5076315
ACS Appl. Mater. Interfaces 2015, 7, 2632–2640

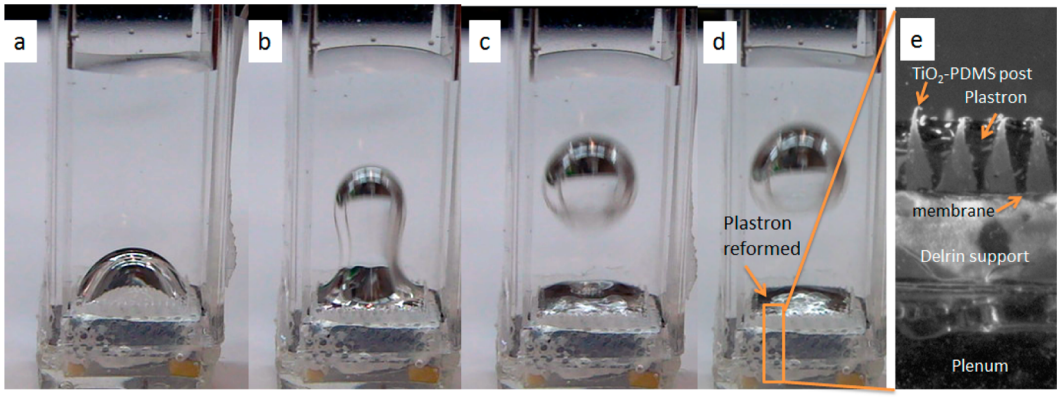

Figure 5. Optical photographs of a TiO_2–PDMS superhydrophobic surface printed on a porous membrane in cuvette photocatalytic reactor, showing the following: (a) gas bubble formed over the surface; (b, c) gas bubble releasing from the surface; (d) plastron layer re-forming with a planar and reflective air–water interface after bubble release; (e) microscope image of TiO_2–PDMS posts printed on Millipore membrane on Delrin plastic over plenum.

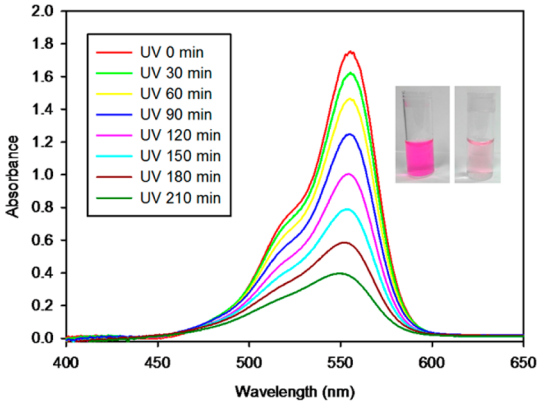

Figure 6. UV–vis spectrum of the RhB solution supported on a TiO_2–PDMS surface in the photoreactor after irradiation times shown in the legend. Inset pictures are the rhodamine B solution before (left) and after (right) UV photodegradation.

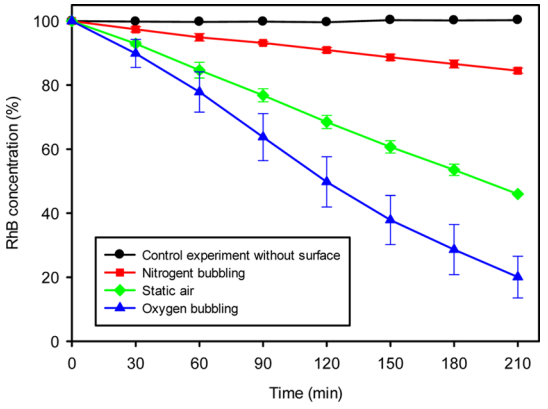

Figure 8. Percent decrease of RhB in an aqueous solution supported on a TiO_2–PDMS superhydrophoibc surface (Cassie state) measured as a function of time under different plastron gas conditions (oxygen bubbling, blue triangle; static air, green diamond; nitrogen bubbling, red square) compared with a control (black circle). At least three experiments were done for each condition.

degradation after 3.5 h of UV irradiation, 76.6 ± 2.6% vs 54.0 ± 0.3% for the RhB solution in the Cassie state. The higher conversion efficiency occurs because of the larger liquid–solid contact area in the Wenzel state compared to the Cassie state, where a plastron layer exists.

To determine if any reactive oxygen species generated in the plastron can be transported into the solution and oxidize the RhB, a capped surface was constructed that physically separates the TiO_2 particles from the aqueous dye solution. On this

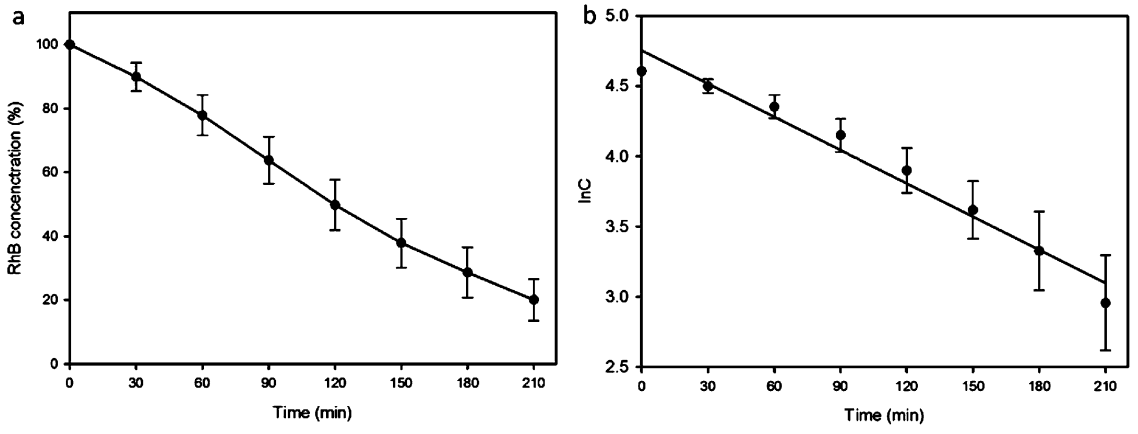

Figure 7. Change in RhB concentration as a function of irradiation time: (a) percent change of RhB concentration decreasing as a function of UV irradiation time; (b) ln of concentration of RhB vs time (rate constant is 0.0079 min^{-1}; R^2 is 0.97).

DOI: 10.1021/am5076315
ACS Appl. Mater. Interfaces 2015, 7, 2632–2640

Table 1. Comparison of Photodegradation Rates of Aqueous Solutions of Dyes in Dispersions with TiO_2 Nanoparticles as Well as in Contact with Hydrophilic and Superhydrophobic TiO_2 Nanocomposite Surfaces

type	composition	dye	light source	catalyst loading (g/L) or surface area (mm^2)	reported k (min^{-1}) × 10^{-3}	k [min^{-1}/(mW/cm^2)] × 10^{-3} normalized
			Type: Superhydrophobic Surface			
superhydrophobic surface	TiO_2 (P-25) coated PDMS[a]	RhB	Dymax Hg lamp, 4 mW/cm^2	8 × 8 mm^2	7.9	2.0
hydrophilic surface	TiO_2–PTFE nanocomposite on Ti[8]	MB	Toshiba high-pressure Hg, 5 mW/cm^2	10 × 10 mm^2	1.1	0.22
			Type: Hydrophilic Surface			
	TiO_2 nanocomposite on Ti[8]	MB	Toshiba high-pressure Hg, 5 mW/cm^2	10 × 10 mm^2	4.7	0.94
			Type: Nanoparticle Dispersion in Aqueous Solution			
nanoparticle dispersion in aqueous solution	P-25[a]	RhB	Dymax Hg lamp, 12 mW/cm^2	5 g/L	38	3.2
	TiO_2–zeolite composite[38]	RhB	320–400 nm, 32 mW/cm^2	6 g/L	~7	0.22
	P-25[39]	RhB	365 nm, 6 W	0.5 g/L	26	

[a]This work.

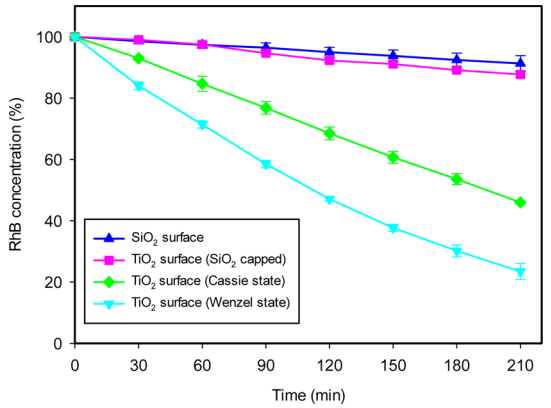

Figure 9. Percent decrease of RhB in an aqueous solution supported on superhydrophobic surfaces (Cassie state) measured as a function of time and as a function of nanoparticle type (TiO_2, green diamond; SiO_2, blue triangle up; SiO_2 capped TiO_2, pink squre). The TiO_2 surface was also measured with the solution in the Wenzel state (cyan triagnle down). At lease three experiments were done for each condition.

capped surface, the tips of the PDMS posts (upper 200 μm) were coated with hydrophobic SiO_2 nanoparticles and the lower part of the PDMS posts were coated with TiO_2 nanoparticles. The photooxidation experiments were conducted under static ambient air conditions (no gas flow through the plastron), and the results are compared with other surfaces in Figure 9.

On the fully coated TiO_2 surface, 54.0 ± 0.3% of the RhB was photooxidized after 3.5 h. However, when TiO_2 particles were isolated from RhB solution, only 12.3 ± 0.9% of the RhB was photooxidized after same UV irradiation time (pink curve in Figure 9). This decrease is similar to the decrease observed on a control surface (8.7 ± 2.5%, blue curve in Figure 9) composed of PDMS posts coated only with SiO_2 nanoparticles. RhB is stable when exposed to UV irradiation (0.3% increase after 3.5 h, black curve in Figure 8, where the increase is due to evaporation of water), a different mechanism must be responsible for the observed decrease in RhB concentration.

The ~10% decrease in RhB observed on SiO_2–PDMS and SiO_2 capped TiO_2 surfaces is due to the absorption of RhB onto the SiO_2 surface as confirmed by optical microscope inspection of the surface after the experiment. Absorption occurs continuously throughout the experiment because the TCL descends slowly into the plastron under UV light, enabling RhB to contact clean nanoparticles on which the dye can absorb. The rounded shape of the SiO_2 capped TiO_2 surfaces creates a higher surface area for RhB absorption which may account for the slightly higher rate (12.3 ± 0.9% vs 8.7 ± 2.5% decrease) on these surfaces relative to the SiO_2 coated PDMS post surface. Because of this absorption of RhB onto the nanoparticle surfaces as well as movement of the triple contact line during the experiment, a contribution from ROS transported across the plastron cannot be ruled out. However, if a high concentration of volatile ROS were formed in the plastron, as observed for Si–phthalocyanine particles,[24] a higher rate of RhB oxidation would be expected.

Self-Cleaning Properties. The TiO_2 surface can photooxidize organics both when in contact with a solution containing the molecules and when the solution is removed leaving the molecules absorbed onto a dry surface. When RhB is absorbed onto the TiO_2–PDMS surface and then dried, UV

DOI: 10.1021/am5076315
ACS Appl. Mater. Interfaces 2015, 7, 2632–2640

irradiation of the dry surface also leads to decoloration as shown in Figure 10. In this dry condition, higher UV power is required for the reaction to proceed, demonstrating the accelerating effect of liquid water on the photooxidation reaction.

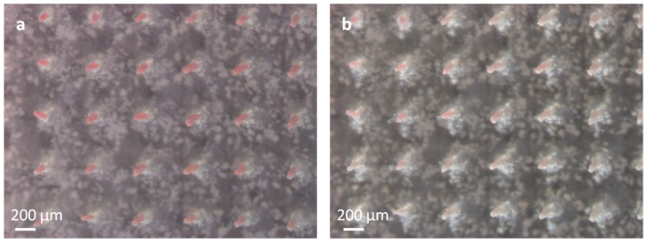

Figure 10. Optical microscope images of RhB coated TiO_2–PDMS posts before and after UV irradiation (200 mW/cm^2 for 2 h): (a) before UV irradiation; (b) after UV irradiation.

Proteins are ubiquitous surface contaminants that can lead to significant changes in surface wettability.[42] To quantify the decomposition of an absorbed protein on a TiO_2–PDMS superhydrophobic surface, a fluorescent protein (bovine serum albumin, Alexa Fluor 488 conjugate) was absorbed onto TiO_2–PDMS and SiO_2–PDMS surfaces. The confocal results show that the TiO_2–PDMS surface (Figure 11a) absorbed more BSA

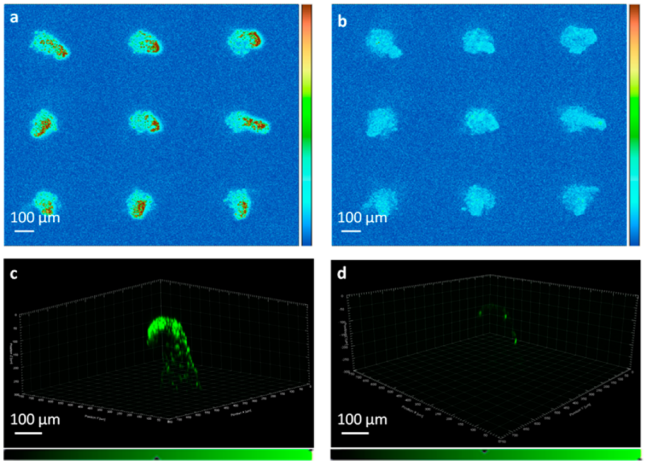

Figure 11. Confocal images of protein coated TiO_2–PDMS posts before and after UV irradiation: (a) top view of protein coated TiO_2–PDMS tips before UV irradiation; (b) top view of tips after UV irradiation; (c) reconstructed 3D image of single post with protein deposition before UV irradiation; (d) 3D image of single post after UV irradiation. Relative fluorescence intensity is shown by color scale on right-hand side of images a and b.

protein than the SiO_2–PDMS surface (Figure 12a). As seen from the 3D reconstructed surface (Figure 11c), the protein absorption on the TiO_2–PDMS surface was limited to the upper 90 μm of the post, which is consistent with the descent of the triple contact line observed in Figure 3. After UV exposure (150 mW/cm^2, 2 h), the integrated fluorescence on the TiO_2–PDMS surface decreased by 91.3% (Figure 11b,d) whereas the fluorescence remained relatively constant on the SiO_2–PDMS surface; the signal degraded by 27.4% (Figure 12b). Color/intensity scales for Figures 11 and 12 are the same, enabling direct comparison of intensities. Photo-oxidation of BSA is not expected on a SiO_2 surface;[43] the decreased

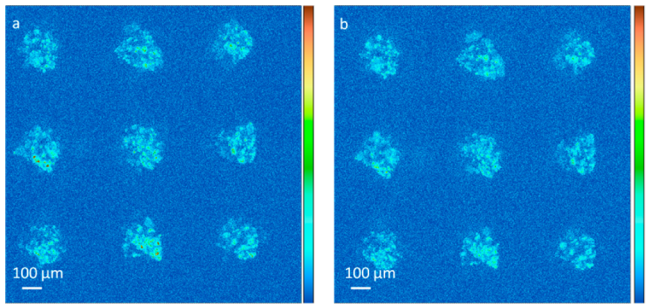

Figure 12. Confocal images of BSA coated SiO_2–PDMS posts before and after UV irradiation: (a) before UV irradiation; (b) after UV irradiation. Relative fluorescence intensity is shown by color scale on right-hand side of images a and b.

fluorescence intensity on the SiO_2–PDMS surface may result from photobleaching of the dye during UV exposure. Although Alexa Fluor 488 is resistant to photobleaching,[44] fluorescence signal degradation is expected upon prolonged irradiation at wavelengths of <500 nm.

These results show that the TiO_2–PDMS surface exhibits robust superhydrophobic and self-cleaning properties. Not only does the surface remain superhydrophobic when exposed to conjugated dyes, protein, and UV light, but the UV light effectively photo-oxidizes absorbed contaminants leading to their removal from the surface.

CONCLUSION

In this paper, we have described a self-cleaning superhydrophobic material where the surface comprises primarily of TiO_2 nanoparticles. The surface remains superhydrophobic, even when the surface of the TiO_2 nanoparticles is rendered hydrophilic. We believe that this is the first example of a superhydrophobic surface, comprising primarily TiO_2, where the Cassie state remains stable after long-term exposure to UV light. The high TiO_2 surface coverage on the PDMS surface results in high catalytic activity; the conjugated dye, rhodamine B, and a BSA protein were efficiently photo-oxidized on the surface.

Hierarchical roughness, ranging from 1 mm tall posts to 20 nm nanoparticles, is responsible for this stability of the plastron. Both optical microscope observations and confocal microscopy on fluorescently tagged BSA confirm that the plastron is stable, descending only ~90 μm after 1.5 h of UV irradiation or 1 h of immersion in protein solution, respectively. No surface modification (e.g., reaction with fluorosilanes) is necessary to maintain a stable plastron layer.

Printing the TiO_2–PDMS superhydrophobic surface on a porous substrate enables facile access to the plastron and control of the gas composition. Because high oxygen concentrations can be maintained at the gas–liquid–solid interface, and the concentration of TiO_2 particles on these superhydrophobic surfaces is large, photooxidation rates of RhB are comparable to hydrophilic TiO_2 nanoparticles dispersed in aqueous solutions.[38,39] These structures provide a unique environment in which photocatalytic mechanistic studies can be conducted as catalyst chemistry, particle size, surface wetting, plastron gas composition, and gas flow rate, can be controlled independently of the aqueous solution composition.

Superhydrophobic materials comprising hydrophilic particles significantly expand the range of potential applications for these nonwetting surfaces. Incorporation of catalytic particles such as

DOI: 10.1021/am5076315
ACS Appl. Mater. Interfaces 2015, 7, 2632–2640

TiO_2 contributes a self-cleaning function to these surfaces which increases their stability when exposed to contaminants (e.g., proteins, dyes, etc.) that cause other superhydrophobic surfaces to transition to a wetted (i.e., Wenzel) state. The fabrication process is inexpensive, easily scalable, and compatible with catalyst particles formed by any synthetic technique. Thus, as TiO_2, or other catalyst chemistries, are modified to increase spectral effeciency,[45] they can be incorporated into these self-cleaning superhydrophobic surfaces, providing a path for further improving their performance.

■ ASSOCIATED CONTENT

Supporting Information

Video of the bubble cycle with gas bubble forming and releasing from the plastron−liquid interface. This material is available free of charge via the Internet at http://pubs.acs.org.

■ AUTHOR INFORMATION

Corresponding Author

*E-mail: alan.lyons@csi.cuny.edu.

Notes

The authors declare no competing financial interest.

■ ACKNOWLEDGMENTS

Y.Z., Y.L., Q.X., M.B., and A.M.L. acknowledge support from the NYS Empire State Development's Division of Science, Technology & Innovation (NYSTAR) and the CUNY Center for Advanced Technology. M.B. also acknowledges support from the National Science Foundation (STEP 0653056). We thank Michael Bucaro for assistance with the SEM imaging and Bikash Mondal for preparation of the protein solution.

■ REFERENCES

(1) Celia, E.; Darmanin, T.; Givenchy, E. T.; Amigoni, S.; Guittard, F. Recent Advances in Designing Superhydrophobic Surfaces. *J. Colloid Interface Sci.* **2013**, *402*, 1−18.

(2) Roach, P.; Shirtcliffe, N. J.; Newton, M. I. Progress in Superhydrophobic Surface Development. *Soft Matter* **2008**, *4*, 224−240.

(3) Crick, C. R.; Parkin, I. P. Preparation and Characterisation of Super-Hydrophobic Surfaces. *Chem.—Eur. J.* **2010**, *16*, 3568−3588.

(4) Feng, X.; Jiang, L. Design and Creation of Superwetting/Antiweting Surfaces. *Adv. Mater.* **2006**, *18*, 3063−3078.

(5) Krupenkin, T. N.; Taylor, J. A.; Wang, E. N.; Kolodner, P.; Hodes, M.; Salamon, T. R. Reversible Wetting-Dewetting Transitions on Electrically Tunable Superhydrophobic Nanostructured Surfaces. *Langmuir* **2007**, *23*, 9128−9133.

(6) Feng, J.; Tuominen, M. T.; Rothstein, J. P. Hierarchical Superhydrophobic Surfaces Fabricated by Dual-Scale Electron-Beam-Lithography with Well-Ordered Secondary Nanostructures. *Adv. Funct. Mater.* **2011**, *21*, 3715−3722.

(7) Shieh, J.; Hou, F. J.; Chen, Y. C.; Chen, H. M.; Yang, S. P.; Cheng, C. C.; Chen, H. L. Robust Airlike Superhydrophobic Surfaces. *Adv. Mater.* **2010**, *22*, 597−601.

(8) Kamegawa, T.; Shimizu, Y.; Yamashita, H. Superhydrophobic Surfaces with Photocatalytic Self-Cleaning Properties by Nanocomposite Coating of TiO_2 and Polytetrafluoroethylene. *Adv. Mater.* **2012**, *24*, 3697−3700.

(9) Ding, X.; Zhou, S.; Gu, G.; Wu, L. A Facile and Large-Area Fabrication Method of Superhydrophobic Self-Cleaning Fluorinated Polysiloxane/TiO_2 Nanocomposite Coatings with Long-Term Durability. *J. Mater. Chem.* **2011**, *21*, 6161−6164.

(10) Xu, Q.; Mondal, B.; Lyons, A. M. Fabricating Superhydrophobic Polymer Surfaces with Excellent Abrasion Resistance by a Simple Lamination Templating Method. *ACS Appl. Mater. Interfaces* **2011**, *3*, 3508−3514.

(11) Xu, Q.; Liu, Y.; Lin, F.-J.; Mondal, B.; Lyons, A. M. Superhydrophobic TiO_2-Polymer Nanocomposite Surface with UV-Induced Reversible Wettability and Self-Cleaning Properties. *ACS Appl. Mater. Interfaces* **2013**, *5*, 8915−8924.

(12) Zhong, W.; Li, Y.; Wang, Y.; Chen, X.; Wang, Y.; Yang, W. Superhydrophobic Polyaniline Hollow Bars: Constructed with Nanorod-Arrays Based on Self-Removing Metal-Monometric Template. *J. Colloid Interface Sci.* **2012**, *365*, 28−32.

(13) Victor, J. J.; Facchini, D.; Erb, U. A Low-Cost Method To Produce Superhydrophobic Polymer Surfaces. *J. Mater. Sci.* **2012**, *47*, 3690−3697.

(14) Yamashita, H.; Nakao, H.; Takeuchi, M.; Nakatani, Y.; Anpo, M. Coating of TiO_2 Photocatalysts on Super-Hydrophobic Porous Teflon Membrane by an Ion Assisted Deposition Method and Their Self-Cleaning Performance. *Nucl. Instrum. Methods Phys. Res., Sect. B* **2004**, *206*, 898−901.

(15) Crick, C. R.; Ismail, S.; Pratten, J.; Parkin, I. P. An Investigation into Bacterial Attachment to an Elastometric Superhydrophobic Surface Prepared via Aerosol Assisted Deposition. *Thin Solid Films* **2011**, *519*, 3722−3727.

(16) Crick, C. R.; Bear, J. C.; Kafizas, A.; Parkin, I. P. Superhydrophobic Photocatalytic Surfaces through Direct Incorporation of Titania Nanoparticles into a Polymer Matrix by Aerosol Assisted Chemical Vapor Deposition. *Adv. Mater.* **2012**, *24*, 3505−3508.

(17) Zhang, X.; Wang, L.; Levänen, E. Superhydrophobic Surfaces for the Reduction of Bacterial Adhesion. *RSC Adv.* **2013**, *3*, 12003−12020.

(18) Tuteja, A.; Choi, W.; Ma, M.; Mabry, J. M.; Mazzella, S. A.; Rutledge, G. C.; McKinley, G. H.; Cohen, R. E. Designing Superoleophobic Surfaces. *Science* **2007**, *318*, 1618−1622.

(19) Cao, L.; Price, T. P.; Weiss, M.; Gao, D. Super Water- and Oil-Repellent Surfaces on Intrinsically Hydrophilic and Oleophilic Porous Silicon Films. *Langmuir* **2008**, *24*, 1640−1643.

(20) Deng, X.; Mammen, L.; Butt, H.-J.; Vollmer, D. Candle Soot as a Template for a Transparent Robust Superamphiphobic Coating. *Science* **2012**, *335*, 67−70.

(21) Paven, M.; Papadopoulos, P.; Schöttler, S.; Deng, X.; Mailänder, V.; Vollmer, D.; Butt, H.-J. Super Liquid-Repellent Gas Membranes for Carbon Dioxide Capture and Heart-Lung Machines. *Nat. Commun.* **2013**, *4*, 2512 DOI: 10.1038/ncomms3512.

(22) Li, J.; Liu, X.; Qiao, Y.; Zhu, H.; Li, J.; Cui, T.; Ding, C. Enhanced Bioactivity and Bacteriostasis Effect of TiO_2 Nanofilms with Favorable Biomimetic Architectures on Titanium Surface. *RSC Adv.* **2013**, *3*, 11214−11225.

(23) Aebisher, D.; Bartusik, D.; Liu, Y.; Zhao, Y.; Barahman, M.; Xu, Q.; Lyons, A. M.; Greer, A. Superhydrophobic Photosensitizers. Mechanisitic Studies of $^1O_2$ Generation in the Plastron and Solid/Liquid Droplet Interface. *J. Am. Chem. Soc.* **2013**, *135*, 18990−18998.

(24) Zhao, Y.; Liu, Y.; Xu, Q.; Barahman, M.; Bartusik, D.; Greer, A.; Lyons, A. M. Singlet Oxygen Generation on Porous Superhydrophobic Surfaces: Effect of Gas Flow and Sensitizer Wetting on Trapping Efficiency. *J. Phys. Chem. A* **2014**, *118*, 10364−10371.

(25) Azimi, G.; Dhiman, R.; Kwon, H.-M.; Paxson, A. T.; Varanasi, K. K. Hydrophobicity of Rare-Earth Oxide Ceramics. *Nat. Mater.* **2013**, *12*, 315−320.

(26) Zhang, F.; Chen, S.; Dong, L.; Lei, Y.; Liu, T.; Yin, Y. Preparation of Superhydrophobic Films on Titanium as Effective Corrosion Barriers. *Appl. Surf. Sci.* **2011**, *257*, 2587−2591.

(27) Sun, W.; Zhou, S.; Chen, P.; Peng, L. Reversible Switching on Superhydrophobic TiO_2 Nano-Strawberry Films Fabricated at Low Temperature. *Chem. Commun.* **2008**, 603−605.

(28) Feng, X.; Zhai, J.; Jiang, L. The Fabrication and Switchable Superhydrophobicity of TiO_2 Nanorod Films. *Angew. Chem., Int. Ed.* **2005**, *44*, 5115−5118.

(29) Kwak, G.; Seol, M.; Tak, Y.; Yong, K. Superhydrophobic ZnO Nanowire Surface: Chemical Modification and Effects of UV Irradiation. *J. Phys. Chem. C* **2009**, *113*, 12085−12089.

DOI: 10.1021/am5076315
ACS Appl. Mater. Interfaces 2015, 7, 2632−2640

(30) Lim, H. S.; Kwak, D.; Lee, D. Y.; Lee, S. G.; Cho, K. UV-Driven Reversible Switching of a Roselike Vanadium Oxide Film between Superhydrophobicity and Superhydrophilicity. *J. Am. Chem. Soc.* **2007**, *129*, 4128−4129.
(31) Jin, R.-H.; Yuan, J.-J. Biomimetically Controlled Formation of Nanotextured Silica/Titania Films on Arbitrary Substrates and Their Tunable Surface Function. *Adv. Mater.* **2009**, *21*, 3750−3753.
(32) Pelaez, M.; Nolan, N. T.; Pillai, S. C.; Seery, M. K.; Falaras, P.; Kontos, A. G.; Dunlop, P. S. M.; Hamilton, J. W. J.; Byrne, J. A.; O'Shea, K.; Entezari, M. H.; Dionysiou, D. D. A Review on the Visible Light Active Titanium Dioxide Photocatalysts for Environmental Applications. *Appl. Catal., B* **2012**, *125*, 331−349.
(33) Barahman, M.; Lyons, A. M. Ratchetlike Slip Angle Anisotropy on Printed Superhydrophobic Surfaces. *Langmuir* **2011**, *27*, 9902−9909.
(34) Lyons, A. M.; Mullins, J.; Barahman, M.; Erlich, I.; Salamon, T. Three-Dimensional Superhydrophobic Structures Printed Using Solid Freeform Fabrication Tools. *Int. J. Rapid Manuf.* **2013**, *3*, 89−104.
(35) Linsebigler, A. L.; Lu, G.; Yates, J. T., Jr. Photocatalysis on TiO_2 Surfaces: Principles, Mechanisms, and Selected Results. *Chem. Rev.* **1995**, *95*, 735−758.
(36) Martin, S. T.; Lee, A. T.; Hoffmann, M. R. Chemical Mechanism of Inorganic Oxidants in the TiO_2/UV Process: Increased Rates of Degradation of Chlorinated Hydrocarbons. *Environ. Sci. Technol.* **1995**, *29*, 2567−2573.
(37) White, M. G. *Heterogeneous Catalysis*; Prentice-Hall Inc.: Englewood Cliffs, NJ, 1990.
(38) You-ji, L.; Wei, C. Photocatalytic Degradation of Rhodamine B Using Nanocrystalline TiO_2-Zeolite Surface Composite Catalysts: Effects of Photocatalytic Condition on Degradation Efficiency. *Catal. Sci. Technol.* **2011**, *1*, 802−809.
(39) Aliabadi, M.; Sagharigar, T. Photocatalytic Removal of Rhodamine B from Aqueous Solutions Using TiO_2 Nanocatalyst. *J. Appl. Environ. Biol. Sci.* **2011**, *1*, 620−626.
(40) Yao, W.; Zhang, B.; Huang, C.; Ma, C.; Song, X.; Xu, Q. Synthesis and Characterization of High Efficiency and Stable Ag_3PO_4/TiO_2 Visible Light Photocatalyst for the Degradation of Methylene Blue and Rhodamine B Solutions. *J. Mater. Chem.* **2012**, *22*, 4050−4055.
(41) Zhang, K.; Oh, W.-C. The Photocatalytic Decomposition of Different Organic Dyes under UV Irradiation with and without H_2O_2 on Fe-ACF/TiO_2 Photocatalysts. *J. Korean Ceram. Soc.* **2009**, *46*, 561−567.
(42) Sigal, G. B.; Mrksich, M.; Whitesides, G. M. Effect of Surface Wettability on the Adsorption of Proteins and Detergents. *J. Am. Chem. Soc.* **1998**, *120*, 3464−3473.
(43) Glazer, A. N.; McKenzie, H. A.; Wake, R. G. The Denaturation of Proteins: II. Ultraviolet Absorption Spectra of Bovine Serum Albumin and Ovalbumin in Urea and in Acid Solution. *Biochim. Biophys. Acta* **1963**, *69*, 240−248.
(44) Panchuk-Voloshina, N.; Haugland, R. P.; Bishop-Stewart, J.; Bhalgat, M. K.; Millard, P. J.; Mao, F.; Leung, W.-Y.; Haugland, R. P. Alexa Dyes, a Series of New Fluorescent Dyes That Yield Exceptionally Bright, Photostable Conjugates. *J. Histochem. Cytochem.* **1999**, *47*, 1179−1188.
(45) Kamegawa, T.; Kido, R.; Yamahana, D.; Yamashita, H. Design of TiO_2-Zeolite Composites with Enhanced Photocatalytic Performances under Irradiation of UV and Visible Light. *Microporous Mesoporous Mater.* **2013**, *165*, 142−147.

DOI: 10.1021/am5076315
ACS Appl. Mater. Interfaces 2015, 7, 2632−2640